Solvation of Na^+ in Argon Clusters

M. Ben El Hadj Rhouma[†]

Laboratoire d'Études des Milieux Ionisés et Réactifs (EMIR), Institut Préparatoire aux Études d'Ingénieurs, Monastir, Tunisia

F. Calvo[‡] **and F. Spiegelman***[,§]

Laboratoire de Chimie et Physique Quantique, IRSAMC, UMR5626 du CNRS, Université Paul Sabatier, 118 route de Narbonne, 31065 Toulouse Cedex 4, France

Received: January 9, 2006; In Final Form: February 20, 2006

The structures and stabilities of Ar_nNa^+ clusters ($n \leq 54$) are investigated using atomistic potentials fitted to reproduce ab initio calculations performed at the coupled-cluster level on the smaller clusters. Polarization effects are described using either the interaction between dipoles induced by the sodium ion, or a small charge transfer in the framework of a fluctuating charges model. In both models, extra three-body contributions of the Axilrod−Teller type are also included between the sodium ion and all pairs of argon atoms. The two models predict essentially similar growth patterns, and a transition in the metal ion coordination from 8 (square antiprism) to 12 (icosahedron) is seen to occur near $n = 50$, in response to the intrasolvent constraints.

I. Introduction

Molecular clusters have attracted significant interest because of their importance in bridging the gap between elementary intermolecular complexes and solvation at the atomic level.[1−4] Neutral clusters are essentially bound by dispersion forces or by weak electrostatic forces if the molecules carry permanent multipoles. They can also be bound by multipole-induced forces such as the hydrogen bond. From a theoretical point of view, molecular clusters have been investigated in terms of their structure, stability, dynamics, and thermodynamics. While ab initio calculations involving perturbative methods (MP2 or MP4) or coupled-cluster approaches are tractable for small clusters, force fields and explicit potentials are still needed for larger species containing more than typically 10 atoms. The celebrated Lennard-Jones (LJ) potential, in particular, has been abundantly employed to study the dynamical or statistical properties of van der Waals clusters.

The situation significantly differs for cationic clusters.[5−12] Indeed, when one constituent is ionized, the leading binding terms become the charged-induced polarization of the other constituents immediately surrounding the ion. The polarization interaction is generally 1 order of magnitude larger than the dispersion forces.[13] For instance, it leads to some important localization in the first shells of helium-doped alkali ions, which are otherwise fluid in the neutral species.[14] Beyond this picture, some charge delocalization can take place and further complicate the situation. In charged homogeneous clusters, delocalization occurs as a resonance process. Conversely, in heterogeneous clusters where the ionization potential of one component is significantly smaller than those of the other components, charge is strongly localized on the former. Ionized Rg_nM^+ clusters (where M is a metal atom cation, and Rg is a rare-gas atom) have recently been investigated both experimentally and theoretically. Lüder and co-workers[6] determined the mass spectra of Rg_nM^+ clusters in time-of-flight experiments. In the case of Ar_nNa^+ clusters, special stabilities at $n = 6$, 8, 10, 13, 16, 20, 23, 25, 26, and 29 were found experimentally, at variance with those obtained for Ar_nK^+ clusters, namely, at $n = 12$, 18, and 22.[6]

These different series of magic numbers were interpreted by Velagrakis et al.[9] in terms of the ratio of the ionic radius versus the van der Waals radius. In this work, the lowest-energy structures were determined from explicit LJ potentials, or by assuming a simple hard-sphere-type construction. Velagrakis and co-workers gave evidence for five successive regimes for the building of the first solvation shell, depending on the radii ratio. Starting with a tetrahedron ($n = 4$), the growth proceeds with an octahedron ($n = 6$), a square antiprism ($n = 8$), a pentagonal antiprism ($n = 10$), and ends with an hexagonal antiprism ($n = 12$). More recently, Hernández-Rojas and Wales[10] carried out the global optimization of Ar_nK^+ and Xe_nCs^+ clusters up to $n = 79$. These authors used potentials more realistic than the bare LJ term, including the long-range Mason−Schamps[15,16] interaction and its $1/R$,[4] $1/R^6$, and $1/R^{12}$ contributions. Icosahedral packing was seen to be dominant for Xe_nCs^+ clusters, which are characterized by radii ratio of 0.84 and special stabilities at $n = 9$, 12, 18, 22, 25, 28, 38, 45, and 48.[10] Conversely, Ar_nK^+ clusters exhibit icosahedral packing only beyond $n = 49$, with the smaller clusters showing enhanced stability at $n = 8$, 15, 19, 21, 31, and 36. For larger sizes, both Xe_nCs^+ and Ar_nK^+ clusters show the same icosahedral stable sizes at $n = 54$, 57, 60, 63, 70, and 73. The transition in Ar_nK^+ is due to the dominance of argon−argon constraints, which scale as the square of the number of solvent rare-gas atoms, whereas the polarization forces behave linearly at a given distance and also decrease as the inverse fourth power of the distance away from the ionized species.

Small Ar_nNa^+ clusters have recently been investigated using ab initio methods[11,12] in the range $n < 10$ with the aim at providing reference results in this small size regime. These

[†] E-mail address: mounir.benrahouma@ipeim.rnu.tn.
[‡] E-mail address: florent.calvo@irsamc.ups-tlse.fr.
[§] E-mail address: fernand.spiegelman@irsamc.ups-tlse.fr.

10.1021/jp060153u CCC: $33.50
Published on Web 03/30/2006

works also quantified the importance of many-body terms in the stability and structure of the small clusters. Nagata et al.[11] performed MP2 calculations and found structures similar to those predicted by Velagrakis for a radii ratio of 0.75 and $n \geq 6$.[9] The disagreement found at smaller sizes ($n < 6$) was interpreted by Nagata et al. as the consequence of many-body forces, particularly the interaction between induced dipoles. Giju et al.[12] also carried out MP2 optimizations with subsequent CCSD(T) single-point energy calculations in the range $n = 2-6$. These authors found different results, especially at sizes of $n = 2$, 3, 4, and 5 for which at least two different isomers were found to have nearly the same energy.

In the present article, we investigate the structure of Ar_nNa^+ clusters in the broader range $n \leq 54$ by parametrizing two many-body models and performing unconstrained global optimization. Our two models differ in their treatment of the polarization interactions. The first scheme considers the perturbative interaction between electrostatic dipoles induced by the sodium ion. In the second model, a partial charge transfer between sodium and the argon atoms is allowed in the framework of self-consistent fluctuating charges.[17,18] In both models, nonadditive overlap effects are also taken into account via an Axilrod−Teller potential between the alkali atom and all pairs of argon atoms. The parametrization was carried out from ab initio calculations at the CCSD(T) level on $ArNa^+$ and Ar_2Na^+ with appropriate correction of the basis set superposition error (BSSE).

II. Models

We now briefly describe the models, which both include pairwise additive terms but differ through the treatment of the many-body polarization effects. These effects are treated via an induced-dipole/induced-dipole model in the first case, and via fluctuating charges in the second case.

A. Pairwise Terms. The potential energy V of the clusters is described in terms of pair-additive functions complemented by a many-body contribution, V_{MB}

$$V = \sum_{j=\mathrm{Ar}} V_{\mathrm{ArNa^+}}(R_{ij}) + \sum_{j,k=\mathrm{Ar}} V_{\mathrm{ArAr}}(R_{jk}) + V_{\mathrm{MB}}$$

where i labels the Na^+ ion, and $j,k = 1...n$ label the argon atoms. V_{ArAr} was taken from Aziz,[19] whereas V_{ArNa^+} was fitted to the ab initio CCSD(T) data including BSSEs via the following expression:

$$V_{\mathrm{ArNa^+}}(R) = aR^c \exp(-bR) - \chi_{\mathrm{pol}}(R)\frac{C_4}{R^4} - \chi_{\mathrm{disp}}(R)\frac{C_6}{R^6}$$

In the above expression, χ_{pol} and χ_{disp} are cutoff functions similar to those introduced by Aziz:[19]

$$\chi(R) = \begin{cases} 1 & \text{if } R > d; \\ \exp\left[-\left(\frac{d}{R} - 1\right)^2\right] & \text{if } R \leq d. \end{cases}$$

The parameters d_{pol} and d_{disp} are the cutoff distances in χ_{pol} and χ_{disp}, respectively.

The many-body interactions stem from different origins, the most important being electrostatic forces. In the present work, two alternative schemes have been used to account for these effects.

B. Induced-Dipole/Induced-Dipole Model. Our first model, denoted as induced dipole/induced dipole (DD) in the following, is perturbative and consists of the interaction between the dipoles on Ar atoms induced by the alkali cation:

$$V_{\mathrm{dip-dip}} = \sum_{j,k=\mathrm{Ar}} \left[\frac{\vec{\mu}_j \cdot \vec{\mu}_k}{R_{jk}^3} - 3\frac{(\vec{\mu}_j \cdot \vec{R}_{jk})(\vec{\mu}_k \cdot \vec{R}_{jk})}{R_{jk}^5} \right] \chi_{\mathrm{dip-dip}}(R_{jk}) \quad (1)$$

with $\vec{\mu}_j$ being the dipole induced on the jth argon atom by the charge located on Na^+, assumed to be $+1$. The value $\vec{\mu}_j$ is calculated using a distance-damped polarizability to avoid divergences at small internuclear distances:

$$\vec{\mu}_j = \alpha_{\mathrm{Ar}} \chi_{\mathrm{pol}}^{1/2}(R_{ij}) \frac{\vec{R}_{ij}}{R_{ij}^3}$$

Similar to the direct polarization interaction between Na^+ and Ar atoms, $\chi_{dip-dip}$ is a damping function of the Aziz type, characterized by the cutoff distance $d_{dip-dip}$.

C. Fluctuating Charges Model. In our second, alternative scheme, the additive polarization of the argon atoms by the sodium ion is complemented by some partial charge transfer, resulting in a nonperturbative Coulomb-type interaction. The fluctuating charges (fluc-q, or FQ model) method,[17] equivalent to the charge equilibration scheme,[18] provides a convenient way of estimating the charges $\{q_i\}$ carried by a set of atoms. Fluc-q potentials have previously been used to model molecules[20] or ions[21] in aqueous solvent. Briefly, the potential V_{fq} is given by

$$V_{\mathrm{fq}} = \sum_i \epsilon_i q_i + \sum_i \frac{H_i}{2} q_i^2 + \sum_{i<j} J_{ij} q_i q_j + \lambda\left(\sum_i q_i - 1\right), \quad (2)$$

where ϵ_i and H_i are the atomic electronegativity and hardness of element $i = Na^+$ or Ar. J_{ij} is the two-center Coulomb integral between elements i and j, which depend on the internuclear distance R through the empirical expression

$$J_{ij} = \left(R^3 + \frac{1}{H_{ij}^3}\right)^{-1/3}$$

At short distances, the Coulomb integral reaches the hardness H_{ij}. To minimize the number of parameters in the model, the hardness between unlike elements is determined according to the simple composition rule $H_{jk} = (H_j + H_k)/2$. In the fluc-q framework, the charges carried by the atoms are obtained self-consistently to minimize the Coulomb energy of the system at the current geometry under the constraint of total charge conservation. This constraint is expressed through a Lagrange multiplier, λ, in eq 2. Because of the self-repulsion quadratic term in V_{fq}, the fluc-q potential does not vanish for infinitely distant atoms, nor do the charges. Unfortunately, this intrinsic behavior of the fluc-q model induces a (small) size-dependent energy shift due to the electronegativity and hardness terms. This is why the total energies given in Tables 2 and 3 are different.

D. Axilrod−Teller Contribution. In addition to the two previous many-body potentials, an extra three-body term is added between the alkali atom and all pairs of argon atoms under the form of an Axilrod−Teller potential.[22] This contribution accounts for three-body overlaps and nonadditive Pauli repulsion effects:

$$V_{\mathrm{AT}} = Z_{\mathrm{AT}} \sum_{j,k=\mathrm{Ar}} \frac{1 - 3\cos(\theta_{ijk})\cos(\theta_{jki})\cos(\theta_{kij})}{R_{ij}^3 R_{ik}^3 R_{jk}^3}$$

TABLE 1: Parameters of the Potentials Used in This Work

	a (Hartree)	b (a_0^{-1})	c (dimensionless)	C_4 (Hartree·a_0^{-4})	C_6 (Hartree·a_0^{-6})	d_{pol} (a_0)	d_{disp} (a_0)
V_{ArNa^+}	24.1744	2.64112	2.92040	5.556	55.9701	6.71353	6.88062
	α_{Ar} (a_0^3)	d_{pol} (a_0)	$d_{dip-dip}$ (a_0)	Z_{AT} (Hartree·a_0^9)			
$V_{dip-dip} + V_{AT}$	11.112	4.57	4.65	548.04			
	$\epsilon_{Na} - \epsilon_{Ar}$ (Hartree)	H_{Na} (Hartree)	H_{Ar} (Hartree)	Z_{AT} (Hartree·a_0^9)			
$V_{fq} + V_{AT}$	0.5607	0.7588	10.0614	2132.13			

TABLE 2: Total Energies (in Hartree) and Symmetry Groups of Ar_nNa^+ Clusters in the DD Model

size	energy	point group	size	energy	point group	size	energy	point group
1	−0.00630	$D_{\infty h}$	19	−0.06650	C_1	37	−0.11109	C_1
2	−0.01241	$D_{\infty h}$	20	−0.06935	C_2	38	−0.11365	C_s
3	−0.01822	C_s	21	−0.07129	C_1	39	−0.11623	C_1
4	−0.02385	C_{2v}	22	−0.07345	C_s	40	−0.11868	C_1
5	−0.02930	C_{4v}	23	−0.07612	C_1	41	−0.12109	C_1
6	−0.03460	O_h	24	−0.07873	C_1	42	−0.12421	C_{2v}
7	−0.03799	C_{3v}	25	−0.08140	C_1	43	−0.12596	C_1
8	−0.04140	D_{4d}	26	−0.08357	C_1	44	−0.12865	C_1
9	−0.04386	C_{4v}	27	−0.08556	C_s	45	−0.13085	C_1
10	−0.04628	D_{4d}	28	−0.08857	C_1	46	−0.13309	C_1
11	−0.04816	C_s	29	−0.09033	C_1	47	−0.13561	C_1
12	−0.05032	C_s	30	−0.09281	C_1	48	−0.13808	C_s
13	−0.05254	C_1	31	−0.09596	C_1	49	−0.13893	C_s
14	−0.05453	C_2	32	−0.09857	C_s	50	−0.14211	C_1
15	−0.05700	C_s	33	−0.10099	C_1	51	−0.14518	C_{3v}
16	−0.05988	C_s	34	−0.10300	C_1	52	−0.14829	C_{2v}
17	−0.06214	C_s	35	−0.10533	C_1	53	−0.15142	C_{5v}
18	−0.06410	C_1	36	−0.10840	C_1	54	−0.15453	C_s

TABLE 3: Total Energies (in Hartree) and Symmetry Groups of Ar_nNa^+ Clusters in the FQ Model, Including the Self-Repulsion Energy (see section II-D)

size	energy	point group	size	energy	point group	size	energy	point group
1	−0.18942	$D_{\infty h}$	19	−0.27455	C_1	37	−0.32601	C_s
2	−0.19757	$D_{\infty h}$	20	−0.27766	C_2	38	−0.32865	C_1
3	−0.20558	C_{2v}	21	−0.28023	C_1	39	−0.33163	C_1
4	−0.21367	D_{4h}	22	−0.28294	C_s	40	−0.33441	C_2
5	−0.22175	C_{4v}	23	−0.28588	C_1	41	−0.33683	C_1
6	−0.22991	O_h	24	−0.28887	C_1	42	−0.34029	C_{2v}
7	−0.23535	C_{3v}	25	−0.29179	C_1	43	−0.34205	C_1
8	−0.24091	D_{4d}	26	−0.29458	C_1	44	−0.34496	C_1
9	−0.24483	C_{4v}	27	−0.29721	C_s	45	−0.34723	C_1
10	−0.24858	D_{4d}	28	−0.30019	C_1	46	−0.34977	C_1
11	−0.25128	C_s	29	−0.30284	C_1	47	−0.35236	C_1
12	−0.25426	C_2	30	−0.30560	C_1	48	−0.35486	C_s
13	−0.25714	C_1	31	−0.30883	C_1	49	−0.35625	C_1
14	−0.25999	C_2	32	−0.31169	C_s	50	−0.35933	C_1
15	−0.26295	C_s	33	−0.31417	C_1	51	−0.36183	C_{3v}
16	−0.26620	C_s	34	−0.31712	C_1	52	−0.36512	C_{2v}
17	−0.26901	C_s	35	−0.31975	C_1	53	−0.36841	C_{5v}
18	−0.27164	C_1	36	−0.32292	C_s	54	−0.37172	I_h

with the index i being kept for the sodium ion. This contribution turned out to be necessary for reproducing the ab initio geometries of the smallest clusters.

III. Results and Discussion

A. Ab Initio Inputs and Parametrization. To parametrize the two models described in the previous section, extensive CCSD(T) calculations were performed on $ArNa^+$ and Ar_2Na^+ using the MOLPRO software package.[23] The variations in the ab initio energy of $ArNa^+$ versus internuclear distance are represented in Figure 1 along with the curves for the two model potentials (DD and FQ). These calculations were carried out using standard semilocal core pseudopotentials, considering one and eight valence electrons outside the core for sodium and argon atoms, respectively. In addition, a core-polarization

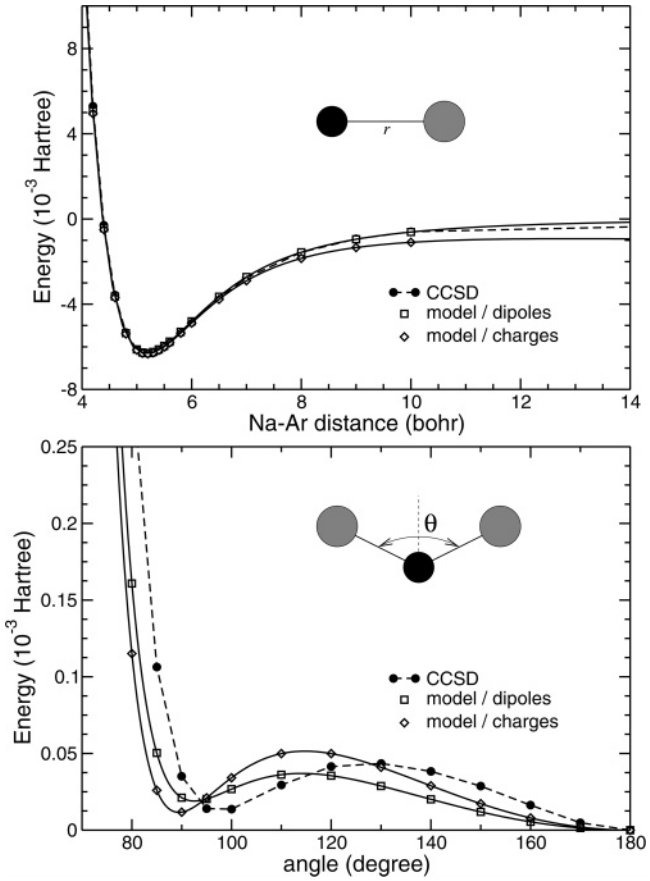

Figure 1. Potential energy curves for $ArNa^+$ and Ar_2Na^+. Upper panel: $ArNa^+$ potential as a function of the internuclear distance from CCSD calculations, and in the DD and FQ models. Lower panel: Ar_2Na^+ potential as a function of the bending angle, at fixed $Ar-Na^+$ distances of 5.20 a_0, from CCSD(T) calculations, and in the DD and FQ models. The curves for the FQ model have been referenced to the minimum energy values.

operator was used on sodium. Extensive uncontracted valence Gaussian-type orbitals basis sets were used, namely, 5s4p3d on sodium and 7s7p5d4f2g on argon. The BSSE was corrected using the counterpoise method by subtracting the energy of the atoms calculated in the total basis for $ArNa^+$. In the case of Ar_2Na^+, the BSSE was thus estimated as

$$\Delta_{BSSE} = 2\Delta_{Ar2Na^+}(Ar) + \Delta_{Ar2Na^+}(Na^+) + 2\Delta_{Ar2Na^+}(ArNa^+) + \Delta_{Ar2Na^+}(Ar_2)$$

where $\Delta_B(A) = E_B(A) - E_A(A)$ is the counterpoise increment energy of fragment A calculated in the larger basis set B. This correction formula thus includes not only the BSSE corrections for atoms in the triatomic basis set, but also that of diatomic fragments in the triatomic basis set. There is no correction for Na^+, which carries no electron. For $ArNa^+$, the results are

extremely close to the highly correlated calculation of Ahmadi et al.[24] who found $D_e = 1300$ cm^{-1} and $R_e = 5.19$ a_0. The present CCSD(T) calculations yield $D_e = 1402$ cm^{-1} without BSSE, 1384 cm^{-1} when the BSSE correction is included, and the same equilibrium distance $R_e = 5.20$ a_0 in both cases. In the case of Ar_2 and after BSSE correction, the ab initio data are in reasonable but not perfect agreement with the experimental values and the empirical adjustments. The BSSE uncorrected dissociation energies ($D_e = 102.3$ cm^{-1}) and the corrected value ($D_e = 82.48$ cm^{-1}), both at $R_e = 7.20$ a_0, are to be compared with the Aziz data of $D_e = 99.78$ cm^{-1} and $R_e = 7.103$ a_0. Despite the rather extensive basis set used here, the discrepancy between the BSSE-corrected result and the Aziz value is still significant. The cause for this discrepancy might be the inadequacy of the BSSE correction using the ghost orbital method for extensive basis sets. We attempted to follow the convergence of the calculated dissociation energy of Ar_2 with increasingly large basis sets. However, we were unable to find any reasonably stable extrapolation scheme. Ab initio data with experimental accuracy on the argon dimer have been reported very recently by Patkowski et al.[25] With respect to the present study, these authors used even larger basis sets on atoms further complemented with midbond functions and a specific extrapolation scheme. However, such a calculation would exceed our present possibilities for Ar_2Na^+.

In Ar_2Na^+, previous authors[11,12] have mentioned a strong competition between a symmetric linear shape ($D_{\infty h}$) and a bent isomer (C_{2v}). In a simple additive potential picture, the Ar_2 intrafragment van der Waals interaction plays a crucial role in the stabilization of the bent isomer. A one-dimensional representation of the potential energy surface of Ar_2Na^+ as a function of the $\widehat{ArNaAr}$ bending angle is given in Figure 1 for the two model potentials as well as for the present CCSD(T) calculations with BSSE corrections. Here we have fixed the two NaAr distances at $R_{NaAr} = 5.20$ a_0. The two $D_{\infty h}$ and C_{2v} minima are quasi degenerate in energy, with the linear isomer being located only 3 cm^{-1} below the C_{2v} isomer, for which the optimal bending angle is about 100°. This value is in agreement with the results by Nagata et al.[11] and by Giju et al.[12] The barrier between the two isomers does not exceed 10 cm^{-1}, and more extensive calculations are probably needed to ascertain which is the lowest isomer, and also to obtain a more accurate estimate of the barrier height. In particular, quantum delocalization is likely to be important. Harmonic estimates with both models provide zero-point energies (ZPEs) at 123 and 132 cm^{-1} with the DD and FQ models, respectively, above the linear isomer. These values are far above the potential barrier separating the two isomers (the ZPE magnitude essentially results from the antisymmetric and symmetric Ar_2Na^+ modes, the ZPE of the $ArNa^+$ diatomic being $\omega_e \approx 60$ cm^{-1}). This should yield a floppy system with a double minimum vibrational ground state in the bending coordinate. A dedicated determination of the anharmonic vibrational ground-state function beyond the harmonic approximation would be very useful, using, for instance, discrete variable representation or diffusion Monte Carlo techniques. This is, however, not the scope of the present paper.

The relative importance of the three-body interactions in Ar_2Na^+ can be inferred from the magnitude of the known Ar_2 interaction. Consistently, using the BSSE-corrected CCSD(T) diatomic data, the differential importance of the three-body contribution in the bending term is estimated to have the same magnitude as the Ar−Ar interaction, that is, around 80 cm^{-1}, to compensate the decrease in the Ar−Ar fragment dispersion contribution in Ar_2Na^+ between $R_{ArAr} \approx 7.20$ a_0 (C_{2v}) and $R_{ArAr} = 10.40$ a_0 (linear).

The parametrization of the DD and FQ models was set to reproduce the ab initio potentials of Figure 1. The Axilrod−Teller parameter Z_{AT} was fitted independently for each model, and the values of all parameters are given in Table 1. The charges were not included as reference data in the fit of the FQ model. It can be noticed that the diatomic curve nearly coincides with the ab initio data close to the equilibrium distance, thus indicating a very small charge transfer. The FQ curve tends to slightly deviate from the reference curve at large distances because of the aforementioned drawback of the FQ model inducing a nonvanishing charge at dissociation. This was actually found to have little effect on the second and third solvation shells.

B. Structures and Energetic Stability. The putative global minima of larger Ar_nNa^+ clusters with $n \leq 54$ were located using the basin-hopping[26] or Monte Carlo+minimization method.[27] For each size n, 10 000 conjugate gradient local minimizations were performed, and random displacements of all atoms were attempted with magnitude of 7 a_0. The temperature in the basin-hopping simulations was set to 100 K.

Figure 2 shows the most stable cluster geometries in the range $n = 3-10$ as well as some remarkable sizes at $n = 16$, 20, 28, 31, 37, 42, 48, 50, 52, and 54. We have not found significant differences between the geometries obtained with the two models, except in the vicinity of $n = 50$ (see below). The symmetry groups and total energies of all clusters are listed in Tables 2 and 3 for the DD and FQ models, respectively.[28]

The results for clusters in the range $n = 3-10$ can be compared with the ab initio results of Nagata et al.[11] and Giju et al.[12] For each size in the range $n = 2-4$, two quasi degenerate isomers are found for both DD and FQ models. For Ar_2Na^+, the global minimum is linear, whereas the bent isomer is slightly higher in energy. It must be emphasized here that the stabilization of the linear isomer is achieved thanks to the many-body terms in our models. The global minimum of Ar_3Na^+ is planar (D_{3h} symmetry group) in both models, but a second three-dimensional isomer with pyramidal C_{3v} symmetry exists, also in both models. For Ar_4Na^+, a competition takes place between the planar D_{4h} isomer and the C_{2v} three-dimensional isomer. While both structures are real minima in the two models, the three-dimensional structure is the global minimum in the DD model, with the planar structure being the lowest in the FQ model.

These results are consistent with those of Giju et al.[12] As already mentioned in previous works, the competition between compact isomers maximizing the number of nearest argon−argon neighbors versus lower dimensionality structures is clearly due to many-body and three-body terms. These isomers do not differ by the number of $ArNa^+$ bonds, but only via their mutual orientation, that is, the balance between the loss of Ar−Ar bonds and the gain in electrostatic many-body energy. In terms of electrostatics, the energy lowering for structures with dipoles pointing outward is favored in the DD model. Equivalently, in the FQ model, the argon atoms gain a small positive charge and tend to avoid each other to some extent. Additionally, the Axilrod−Teller three-body interactions, with $Z_{AT} > 0$ in both models, further favor open structures. The many- and three-body contributions of the DD and FQ potentials thus stabilize the linear or planar structures versus more compact shapes. This effect must of course be scaled against the number of Ar−Ar interactions, hence it becomes less influential on the structures for $n > 4$. In the range $n = 5-8$, all global minima are three-

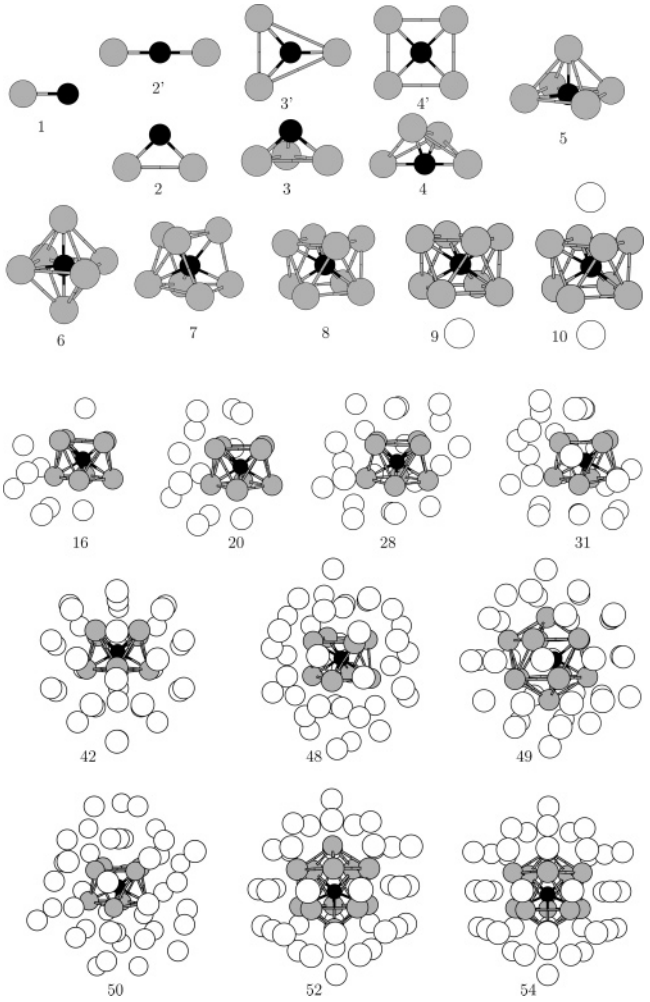

Figure 2. Lowest-energy isomers of Ar_nNa^+ clusters for selected sizes $n = 1-10$, 16, 20, 28, 31, 42, 48, 49, 50, 52, and 54, obtained with the DD model. Two nearly degenerate isomers are shown for sizes $n = 2-4$.

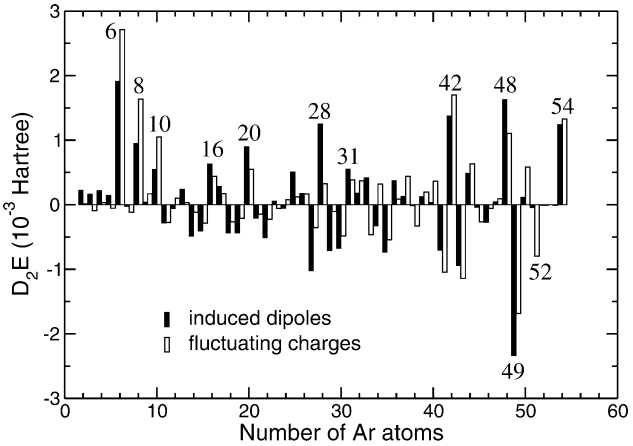

Figure 3. Second energy difference $\Delta_2E(n) = E(n + 1) + E(n - 1) - 2E(n)$ versus size n within the DD and FQ models.

dimensional, in agreement with the results of Giju et al.[11] and Nagata et al.[12]

The second energy difference $\Delta_2E(n) = E(n + 1) + E(n - 1) - 2E(n)$ between size n and its immediate neighbors usually emphasizes the particularly stable sizes with respect to their immediate neighbors. The variations of Δ_2E with n are shown in Figure 3 for the two models. Sizes 6 and 8 are especially prominent: they correspond to isomers with particularly high symmetries, maximizing the number of $Ar-Na^+$ and Ar−Ar interactions at optimal distances in the first solvation shell. Clear extrema are also seen at $n = 20$, 28, 42, 48, and 54. Even though the magic sizes are generally more pronounced in the FQ model, very few qualitative differences are found between the DD and FQ models, except at $n = 52$. This size lies near the structural transition of the first solvation shell, but differs somewhat in the two models because of some nontrivial cluster size effects and the large number of quasi degenerate isomers. In the range $n = 49-52$, the lowest isomers with an 8-coordinated first shell and those with coordination 12 are very close in energy, and their ordering changes slightly with the model chosen.

The selected clusters in Figure 2 illustrate the two main growth regimes of Ar_nNa^+ clusters. The completion of the very stable square antiprism occurs at $n = 8$, with all argon atoms being located at 5.20 a_0 from the alkali ion. Capping this structure twice above the squares leads to another stable cluster at $n = 10$, with the two extra atoms at 8 a_0 from the ion. Above this size, argon atoms are added in capping positions, but the filling of external shells is not centered on the ion until about 40 argon atoms are present. The usual polyicosahedral growth of pure argon clusters[29,30] is hindered by the square antiprism core, and this effect of geometric frustration strongly reduces the overall ordering of the argon layers. Most of the specially stable sizes, as inferred from the extrema in the second energy derivative plot, do not exhibit a strong ordering, and only in very few cases ($n = 42$ and 54) does the global minimum have a significant symmetry. The low symmetry of most structures probably results from the presence of many-body and three-body terms in the models. Interestingly, the global minima reported by Hernández-Rojas and Wales, obtained from pure pair potentials, usually exhibit higher symmetry, even for rather large sizes.[10]

Once a sufficient number of argon atoms have been added, the argon−argon constraints stabilize the multilayer icosahedral structures found in pure rare-gas clusters.[30,31] The alkali ion exerts a lesser influence on the overall shape of the cluster, especially near the onset of the shell closure at $n = 54$. In the DD model, because of the different equilibrium distances in Ar_2 and $ArNa^+$, the alkali ion is not located in the center of the icosahedral solvent shell for $n \geq 50$. The distortion of the alkali from the icosahedron center can reach about 1 a_0. In the FQ model, the interactions are more isotropic, and the I_h symmetry is conserved. Because of the core structural transition, no extra shell around the square antiprism is seen. The present results are consistent with those of Hernández-Rojas and Wales,[10] who found a transition from 8-coordinated to 12-coordinated alkali ions in similar Ar_nK^+ clusters, also near 50 rare-gas atoms.

C. Energetic Contributions to the Models. The different energetic contributions to the many-body DD potential are represented in Figure 4. The completion of the first solvation shell clearly has an energetic signature, as the Ar_n-Na^+ contribution reaches a saturation value near $n = 10$. This can be roughly rationalized as being due to the linear increase of the polarization contributions in the first shell with the number of argon atoms. The saturation of this direct polarization energy occurs once this shell is completed, since each term goes as the inverse fourth power of the $Ar-Na^+$ distance. Up to $n \simeq 10$, the interaction among argon atoms nearly compensates the electrostatic interaction between induced dipoles. We also note that the three-body Axilrod−Teller contribution has a much smaller magnitude than the other terms. This term turns out to be important only for stabilizing the open structures of the smallest clusters.

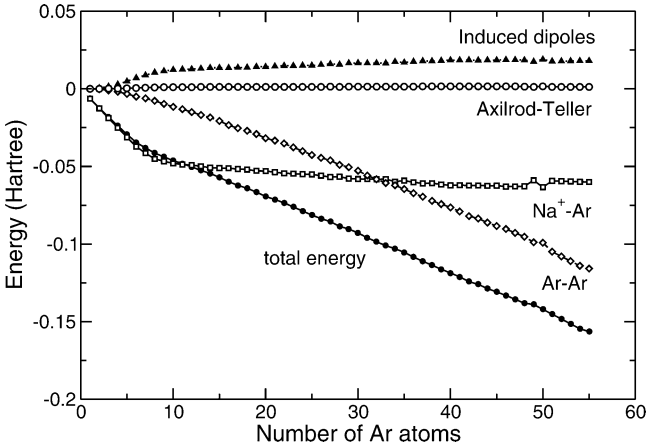

Figure 4. The different energy contributions in the total binding energy of Ar_nNa^+ clusters in the DD model.

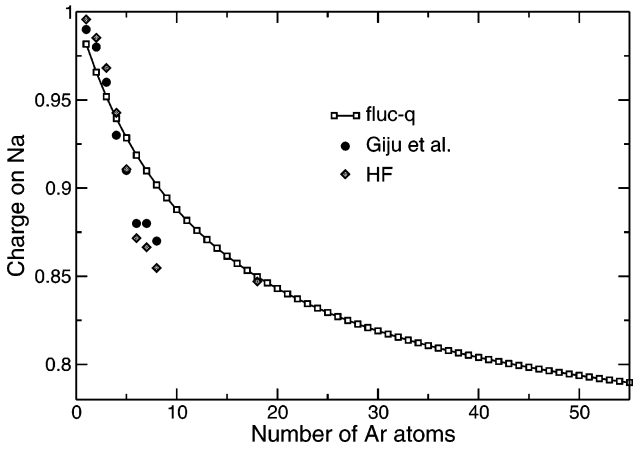

Figure 5. Charge transfer on sodium in Ar_nNa^+ clusters within the FQ model. The ab initio MP2 results of Giju and co-workers,[12] as well as the present Hartree−Fock data, are represented for specific sizes.

Focusing now on the FQ model, Figure 5 shows the variations of the effective charge carried by the alkali ion as a function of the number of surrounding argon atoms. For comparison, we have also given the CCSD(T) charges obtained by Giju et al. calculated up to $n = 8$,[12] as well as the Hartree−Fock charges for the same clusters computed here. A complementary calculation was performed for the D_{4d} structure of $Ar_{18}Na^+$ resulting from capping the eight triangular facets of the first shell of Ar_{10}-Na^+, which was locally optimized. We stress here that the charges obtained with the FQ model were not part of the fitting procedure, but are an independent outcome.

The charge decreases monotonically with the number of argon atoms, in agreement with the first-principles calculations, for which the Hartree−Fock and MP2 results also agree with each other. Charge transfer is rather underestimated in the range $n = 5-10$, but agrees very well at size $n = 18$. The ab initio data seem to show that charge transfer essentially stops after the completion of the first solvation shell. The fluc-q model behaves much more smoothly, mainly because of the long range of the Coulomb interaction and the ignoring of real chemical bonds. An important result is that charge transfer is indeed significant and reaches about 0.2 electrons in the limit of large clusters.

IV. Conclusion

The present work confirms the preference of positively charged metal atoms in a rare-gas solvent for ion-centered structures. We have developed two different atomistic potentials, including pairwise, three-body, and many-body contributions to study the structure of clusters containing up to several tens of rare-gas atoms. These potentials were carefully fitted using dedicated ab initio calculations performed at the CCSD(T) level. Terms beyond the pair interactions appear to be essential for stabilizing the linear or planar global minima that are predicted by ab initio calculations. The two models represent the many-body polarization effects either from the interaction between electric dipoles induced by the alkali cation, or from a partial charge transfer between unlike elements through the fluctuating charges framework. The putative lowest-energy structures found by both models show a transition from a square antiprism, 8-coordinated first solvation shell below $n \simeq 50$ toward a 12-coordinated icosahedral shell above this size. This transition is induced by the intra-argon constraints. As long as magic numbers are actually being governed by geometric structure, the present investigation agrees well with experimental data,[6] except in the size range $n = 23-29$, which was not reproduced here. An explanation could lie in the very floppy character of the second shell and the possible finite temperature or entropic effects. Indeed the influence of temperature on mass spectrometry and magic numbers has previously been observed by Branz et al. in $(C_{60})_n$ clusters.[33]

Even though they include contributions beyond the pair terms, the present models could be exploited to investigate other dynamical properties, even for large clusters or bulk systems. In fact, the induced dipoles and Axilrod−Teller potentials convey the same numerical cost as a pair potential, because they only involve all pairs of argon atoms. In the case of the fluc-q potential, significant savings are achieved by treating the partial charges as independent variables in molecular dynamics simulations.[17]

The most stable structures of Ar_nNa^+ clusters will be influenced by at least two other effects that would require special examination. First, as seen here for $n = 2$, zero-point effects and quantum vibrational delocalization might be of importance for the smallest clusters, for which very small frequencies and/or shallow wells are found. Such effects are known to be crucial for ions solvated in helium atoms, but could also be responsible for some structural changes in the present, heavier systems. Quantum diffusion Monte Carlo simulations would be a convenient way to proceed in order to take these effects into account. Even at the simplest harmonic level, ZPEs could delay the transition of the first solvation shell between the square antiprism and the icosahedron because the latter is less tightly bound to the alkali than the former, possibly resulting in lower vibrational frequencies.

Second, temperature effects could also play a role in favoring conformations, which are not the lowest in energy. Again, structures with lower vibrational frequencies will benefit from a slight increase in temperature. Both quantum delocalization and temperature effects are included in the inherent structure picture of the potential energy surfaces, which we previously applied to neutral $CaAr_n$ clusters.[32]

Finally, the stability and structure of mixed charged cluster ions are also of interest in the context of excited states in the neutral species.[34−36] As an electron of the neutral cluster is promoted to more and more diffuse excited orbitals, a Rydberg-type situation may be reached. This would correspond here to a sodium ion solvated by an argon shell, with an excited electron orbiting beyond the argon shell. A strong interplay between cluster size, geometric structure, and excitation level is expected. Work is currently in progress to address this issue.[37]

References and Notes

(1) Halberstadt, N.; Janda, K. *Dynamics of van der Waals Complexes*; NATO ASI series; Plenum Press: New York, 1990; Vol. 227, p 471.

(2) Zewail, A. H. *Femtochemistry: Ultrafast Dynamics of the Chemical Bond*; World Scientific: Singapore, 1994; Vols. I and II.

(3) Breckenridge, W. H.; Jouvet, C.; Soep, B. Metal-Atom/Rare-Gas van der Waals Complexes. In *Advances in Metal Semiconductors and Clusters*; Duncan, M. A., Ed.; JAI Press Inc.: Greenwich, CT, 1995; Vol. 3.

(4) Chergui, M. *Femtochemistry: Ultrafast Chemical and Physical Processes in Molecular Systems*; World Scientific: Singapore, 1996.

(5) Lüder, C.; Velagrakis, M. *J. Chem. Phys*. **1996**, *105*, 2167.

(6) Lüder, C.; Prekas, D.; Velagrakis, M. *Laser Chem.* **1997**, *17*, 109.

(7) Prekas, D.; Lüder, C.; Velagrakis, M. *J. Chem. Phys.* **1998**, *108*, 4450.

(8) Froudakis, G. E.; Farantos, S. C.; Velagrakis, M. J. *J. Chem. Phys*. **2000**, *258*, 13.

(9) Velagrakis, M. *Adv. Met. Semicond. Clusters* **2001**, *5*, 227.

(10) Hernández-Rojas, J.; Wales, D. J. *J. Chem. Phys*. **2003**, *119*, 7800.

(11) Nagata, T.; Ayoagi, M.; Iwata, S. *J. Phys. Chem. A* **2004**, *108*, 683.

(12) Giju, K. T.; Roszack, S.; Gora, R. W.; Leszczynski, J. *Chem. Phys. Lett*. **2004**, *391*, 112.

(13) Bellert, D.; Breckenridge, W. H. *Chem. Rev.* **2002**, *102*, 1595.

(14) Di Paola, C.; Sebastianelli, F.; Bodo, E.; Baccarelli, I.; Gianturco, F. A. *J. Chem. Theory Comput*. **2005**, *1*, 1045.

(15) Mason, E. A.; Schamps, H. W. *Ann. Phys. (NY)* **1958**, *4*, 233.

(16) Jones, J. E.; Ingham, A. E. *Proc. R. Soc. London, Ser. A* **1925**, *107*, 636.

(17) Rick, S. W.; Stuart, S. J.; Berne, B. J. *J. Chem. Phys*. **1994**, *101*, 6141.

(18) Mortier, W. J.; Genechten, K. V.; Gasteiger, J. *J. Am. Chem. Soc*. **1985**, *107*, 829. Rappé, A. K.; Goddard, W. A., III *J. Phys. Chem*. **1991**, *95*, 3358.

(19) Aziz, R. A.; Chen, H. H. *J. Chem. Phys*. **1977**, *67*, 5719.

(20) Rick, S. W.; Stuart, S. J.; Bader, J. S.; Berne, B. J. *J. Mol. Liq.* **1995**, *65/66*, 31.

(21) Clavaguéra, C.; Calvo, F.; Dognon, J.-P. *J. Chem. Phys.* **2006**, *124*, 074505.

(22) Axilrod, B. M.; Teller, E. *J. Chem. Phys*. **1943**, *11*, 299.

(23) Werner, H.-J.; Knowles, P. J.; Amos, R. D.; Bernhardsson, A.; Berning, A.; Celani, P.; Cooper, D. L.; Deegan, M. J. O.; Dobbyn, A. J.; Eckert, F.; Hampel, C.; Hetzer, G.; Knowles, P. J.; Korona, T.; Lindh, R.; Lloyd, A. W.; McNicholas, S. J.; Manby, F. R.; Meyer, W.; Mura, M. E.; Nicklass, A.; Palmieri, P.; Pitzer, R.; Rauhut, G.; Schtz, M.; Schumann, U.; Stoll, H.; Stone, A. J.; Tarroni, R.; Thorsteinsson, T. *MOLPRO*, version 2002.1; Cardiff University: Wales, UK, 2002.

(24) Ahmadi, G. R.; Reggen, I. *J. Phys. B: At. Mol. Opt. Phys*. **1994**, *27*, 5603.

(25) Patkowski, K. Murdachaev, G.; Fou, C. M.; Szalewisz, K. **2005**, *103*, 2031.

(26) Wales, D. J.; Doye, J. P. K. *J. Phys. Chem. A* **1997**, *101*, 5111.

(27) Wales, D. J.; Scheraga, H. A. *Science* **1999**, *285*, 1368.

(28) Isomer geometries with both DD and FQ models for all sizes $n \leq 54$ are available upon request to the authors.

(29) Farges, J.; de Feraudy, M.-F.; Raoult, B.; Torchet, G. *J. Chem. Phys*. **1983**, *78*, 5067.

(30) Northby, J. A. *J. Chem. Phys*. **1987**, *87*, 6166.

(31) Farges, J.; de Feraudy, M.-F.; Raoult, B.; Torchet, G. *J. Chem. Phys*. **1986**, *84*, 3491.

(32) Calvo, F.; Spiegelman, F.; Heitz, M.-C. *J. Chem. Phys*. **2003**, *118*, 8739.

(33) Branz, W.; Malinowski, N.; Schaber, H.; Martin, T. P. *Chem. Phys. Lett*. **2000**, *328*, 245.

(34) Tutein, A. B.; Mayne, H. R. *J. Chem. Phys*. **1998**, *108*, 308.

(35) Fujisaki, A. *J. Chem. Phys.* **2002**, *117*, 5271.

(36) Ben El Hadj Rhouma, M.; Ben Lahkhdar, Z.; Spiegelman, F. In *Advances in the Theory of Chemical and Physical Systems*; Springer Series in Theoretical Chemistry and Physics; Springer-Verlag: Berlin, 2006; Vol. XV, p 450.

(37) Ben El Hadj Rhouma, M.; Ben Lahkhdar, Z.; Spiegelman, F. To be submitted for publication.